Experimental setup for temporally and spatially resolved ICCD imaging of (sub)nanosecond streamer plasma

Document Version:
Publisher's PDF, also known as Version of Record (includes final page, issue and volume numbers)

Please check the document version of this publication:

• A submitted manuscript is the version of the article upon submission and before peer-review. There can be important differences between the submitted version and the official published version of record. People interested in the research are advised to contact the author for the final version of the publication, or visit the DOI to the publisher's website.
• The final author version and the galley proof are versions of the publication after peer review.
• The final published version features the final layout of the paper including the volume, issue and page numbers.

[Link to publication](#)

Experimental setup for temporally and spatially resolved ICCD imaging of (sub)nanosecond streamer plasma

T. Huiskamp, W. Sengers, and A. J. M. Pemen

Experimental setup for temporally and spatially resolved ICCD imaging of (sub)nanosecond streamer plasma

T. Huiskamp,[a)] W. Sengers, and A. J. M. Pemen
*Eindhoven University of Technology, Electrical Engineering, Electrical Energy Systems Group,
5600MB Eindhoven, The Netherlands*

Streamer discharges are efficient non-thermal plasmas for air purification and can be generated in wire-cylinder electrode structures (the plasma reactor). When (sub)nanosecond high-voltage pulses are used to generate the plasma, components like a plasma reactor behave as transmission lines, where transmission times and reflections become important. We want to visually study the influence of these transmission-line effects on the streamer development in the reactor. Therefore, we need a unique experimental setup, which allows us to image the streamers with nanosecond time resolution over the entire length of the plasma reactor. This paper describes the setup we developed for this purpose. The setup consists of a large frame in which a specially designed plasma reactor can be mounted and imaged from below by an intensified charge-coupled device (ICCD) camera. This camera is mounted on a platform which can be moved by a stepper motor. A computer automates all the experiments and controls the camera movement, camera settings, and the nanosecond high-voltage pulse source we use for the experiments. With the automated setup, we can make ICCD images of the entire plasma reactor at different instances of time with nanosecond resolution (with a jitter of less than several hundreds of picoseconds). Consequently, parameters such as the streamer length and width can be calculated automatically. *Published by AIP Publishing.* [http://dx.doi.org/10.1063/1.4972413]

I. INTRODUCTION

Recently, we developed high-voltage (sub)nanosecond pulsed power technology in order to generate transient plasma for air purification applications.[1–4] This transient plasma consists of multiple parallel filaments called streamers. These streamers typically have a velocity in the range of 10^5 -10^7 m · s^{-1} and a diameter of several hundred micrometers to several millimeters.[5–15] Due to the high energetic electrons that are generated in these non-thermal plasmas, they are very efficient in producing highly reactive radical species.[16,17] These species can consequently react with, for instance, particles in gas streams (for example, pollutants, odor and dust), contamination in water, biological tissue, and material surfaces.[16,18] In our research, we mainly consider transient plasma for air-purification applications.[19]

Previous research shows that non-thermal plasma generated by very short (nanosecond) high-voltage pulses is very efficient for a variety of applications.[20–27] Overall, researches have noted that the pulse duration of the applied high-voltage pulse has a significant influence on the radical yield of the transient plasmas generated with these pulses; shorter pulses result in higher yields.[20–22,26] To study and understand this phenomenon, we developed a nanosecond pulse source that produces even shorter and faster pulses than realized by other research groups. The output pulses from this nanosecond pulse source have an adjustable amplitude of up to 50 kV (positive and negative), an adjustable pulse duration of 0.5–10 ns, and a rise time of less than 200 ps.

Streamer discharges can be generated in wire-cylinder electrode structures (the plasma reactor), where the high-voltage pulses are applied to the wire electrode. Such a discharge is also called a pulsed corona discharge. When (sub)nanosecond pulses are used, components like a plasma reactor behave as transmission lines, where transmission times and reflections become important. Therefore, the development and propagation of the streamers will be dictated by the pulse propagation and reflections in the reactor. Consequently, the streamer development changes on very short time scales and will be dependent on the position in the reactor. For example, a 1-ns pulse is only 30 cm "long" in air if we assume that the pulse propagates with the speed of light in the reactor, while typical plasma reactor lengths are of the order of 1 m. We want to visually study the influence of these transmission-line effects on the streamer development in the reactor. Therefore, we need a unique experimental setup, which allows us to image the streamers with nanosecond time resolution over the entire length of the plasma reactor. This paper describes this setup.

II. SETUP DEVELOPMENT AND PROCEDURE

As stated in the Introduction, the streamer development in our pulsed corona-plasma reactor depends on the propagation of the very short pulses through the reactor. Therefore, we need to be able to visualize the streamers both as a function of time as well as a function of position in the reactor. The temporal development of the streamer propagation is recorded by imaging the streamer discharge at multiple instances in time with an ICCD (intensified charge-coupled device) camera. However, if we capture the whole reactor in one image, the resolution of the images is inadequate to distinguish individual

---
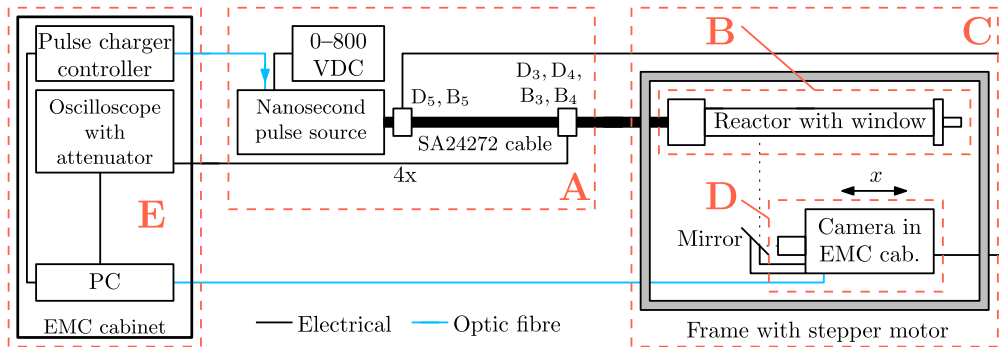
a)Electronic mail: t.huiskamp@tue.nl

FIG. 1. A schematic of the automated experimental setup: (A) the nanosecond pulse source, (B) the plasma reactor, (C) the camera frame, (D) the movable camera system, and (E) the shielded (EMC) cabinet with controls and oscilloscope. A computer controls the camera and the camera position via optic fibre. For each photo the computer generates a pulse with the pulse source and records the waveforms from D-dot sensors, D_3 and D_4 and B-dot sensors, B_3 and B_4 from the oscilloscope.

streamers and calculate their properties. Therefore, we move the camera during the experiment to capture images at multiple positions in the reactor and later stitch these images together to generate an overview of the entire reactor. This results in a significant amount of measurements and data, which is why the experiments will be automated. Furthermore, the camera is mounted on a motorized, movable platform that can be automatically controlled by software.

Figure 1 shows the entire experimental setup. It consists of five main parts, which will be described in detail in Secs. II A–II F:

A: The nanosecond pulse source and sensors.
B: The plasma reactor.
C: The camera frame.
D: The movable camera system.
E: The shielded cabinet with controls and oscilloscope.

A. Nanosecond pulse source and sensors

The nanosecond pulse source which we used for the experiments in this paper was recently developed at the Eindhoven University of Technology. It is a single line pulse source, consisting of a pulse forming line (PFL) that is charged by a microsecond pulse charger and is subsequently discharged by an oil spark gap. The generated pulses then travel over a transmission line (a SA24272 coaxial cable) to the load, the corona reactor, where they produce such a high electric field that a streamer discharge develops. (The coaxial cable adds a delay to the high-voltage pulses and is required to synchronize the ICCD camera with the generated high-voltage pulses.) The full design of this system is described in Refs. 1–4 and is schematically presented in Fig. 2. The output pulses from

this nanosecond pulse source (50 Ω output impedance) have an adjustable amplitude of 3–50 kV (positive and negative), an adjustable pulse duration of 0.5–10 ns, and a rise time of less than 200 ps. Figure 3 shows some example waveforms.

With a pulse-charger controller and a DC power supply, we control the pulse charger and therefore the charging voltage and amplitude of the nanosecond pulse source. The pulse repetition rate and the charge time of the switches of the pulse charger are also controlled by the pulse-charger controller, which is located in a shielded cabinet (connected via optic fibre). This controller

(a)

(b)

FIG. 3. Example waveforms of the nanosecond pulse source. (a) An 8-ns pulse with different amplitudes. (b) A 22-kV pulse with different pulse durations (from 0.5 to 10 ns).
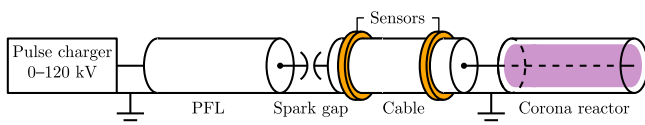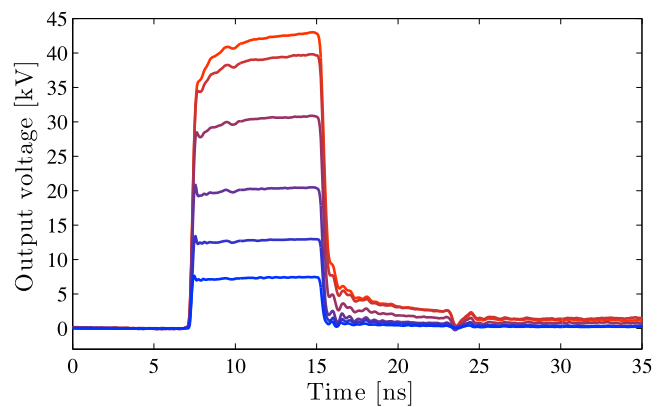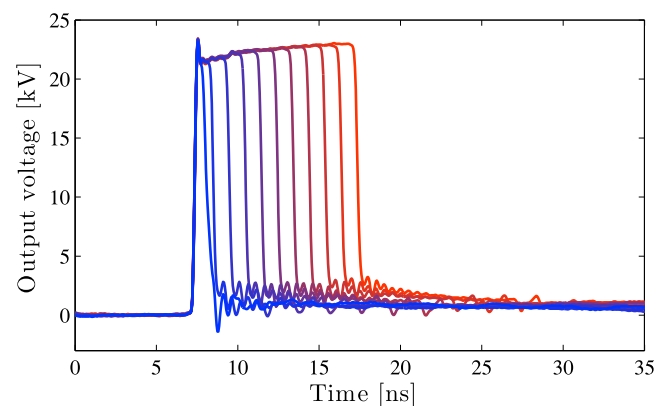

FIG. 2. Schematic of the single line pulse source. The pulse charger charges the pulse forming line (PFL) which is then discharged by the spark gap into a matched cable. When the voltage pulse reaches the corona reactor, it generates a corona discharge. B-dot and D-dot sensors are integrated on the cable for current and voltage measurements.
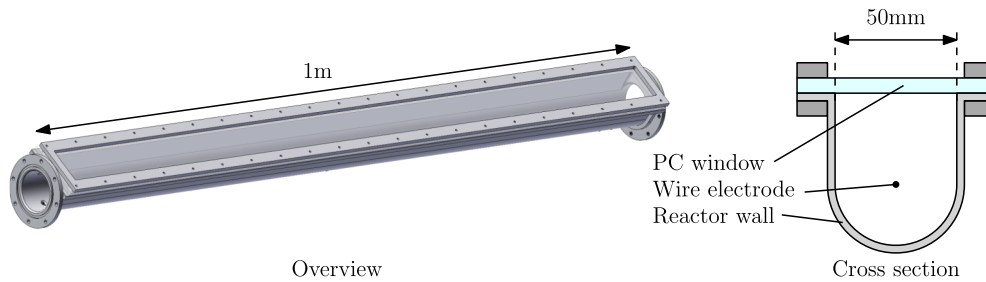
FIG. 4. An overview drawing of the 1-m corona-plasma reactor with a polycarbonate window (left) and a cross section of this reactor (right). The reactor has a U-shaped cross section that allows the ICCD camera to image the inside of the reactor. Two of these 1-m reactors can be connected in series to obtain a 2-m long reactor.

can be controlled by a computer over a RS232 connection. We will give more information on the entire control structure of the experimental setup in Section II E.

The pulse source is connected to the plasma reactor by a SA24272 coaxial cable. On this cable we mounted B-dot and D-dot sensors to measure the current and voltage of the high-voltage pulses, respectively.[28] Four sensors are mounted on the side of the plasma reactor (D_3, D_4, B_3, and B_4) and two on the pulse source side (D_5 and B_5). For example, the waveforms of Fig. 3 were measured with sensor D_5.

B. Plasma reactor

The plasma reactor is connected to the end of the SA24272 coaxial cable. This connection is made with a cable coupler, that was designed to be impedance matched to the coaxial cable and was introduced in Ref. 29.

Normally, we use a coaxial plasma reactor for a homogenous electric field distribution. However, for our imaging experiments we require good optical access to the streamer discharge. Therefore, we used a plasma reactor that has a window along its entire length but is in every other way similar to the coaxial reactor. Figure 4 shows this reactor. It is 1 m long and two of these reactors can be connected in series to create

a 2-m long reactor. The reactor has a gas-tight polycarbonate (PC) window to allow imaging of the streamer discharge. The U-shaped reactor can be connected to the cable coupler on the SA24272 cable in the same way as our normal coaxial reactor.

If we want to use the imaging results with the U-shaped reactor to explain observations from electrical and chemical measurements in our normal coaxial reactor, we need to examine the differences between these reactors. We already mentioned that the U-shaped reactor was designed to be as similar as possible as the coaxial reactor. They have the same diameter, the same length, and use the same cable coupler and wire-tightening mechanism. Furthermore, a simulation of the electric field distribution with CST Microwave Studio shows that the electric field distribution inside the U-shaped reactor is very similar to the electric field distribution in the coaxial reactor. Figure 5 shows this simulation result. Especially around the wire, the electric field distribution is very similar to that of a coaxial reactor. If the electric field distribution is similar, the streamer inception and development will also be very similar.

Despite the similarities between the reactors, the streamers will not propagate directly towards the ICCD camera because there is no counter-electrode in that direction. Therefore, it is likely that (slightly) less streamers are generated in the U-shaped reactor and therefore the dissipated plasma energy is lower. Figure 6 shows this dissipated plasma energy for both a cylindrical reactor and our U-shaped reactor. This plasma energy was measured with B-dot and D-dot sensors, D_3, D_4,
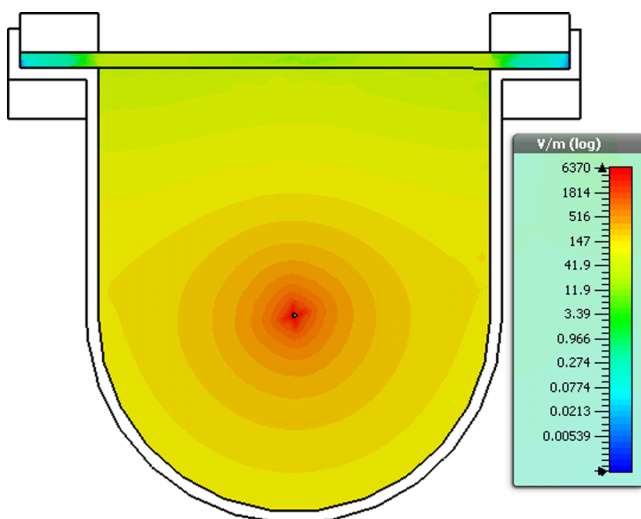
FIG. 5. A simulation of the electric field distribution in the U-shaped reactor. Positive voltage is applied to the center electrode and the outer electrode is grounded. The result shows a very similar electric field distribution that would be present in a coaxial reactor.
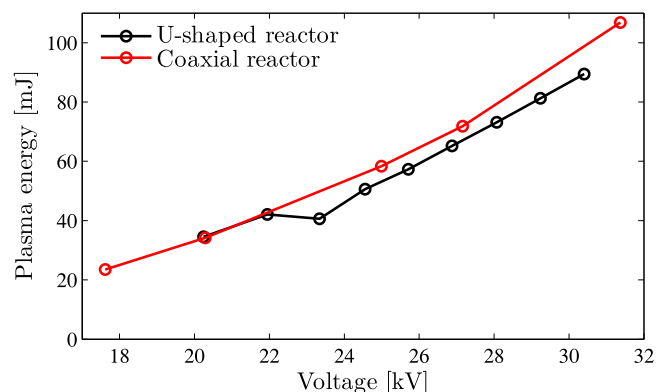
FIG. 6. The difference in the dissipated plasma energy as a function of voltage for the U-shaped reactor that we used in the experimental setup of this paper and the coaxial reactor we normally use. The results are very similar with a slightly lower plasma energy for the U-shaped reactor.
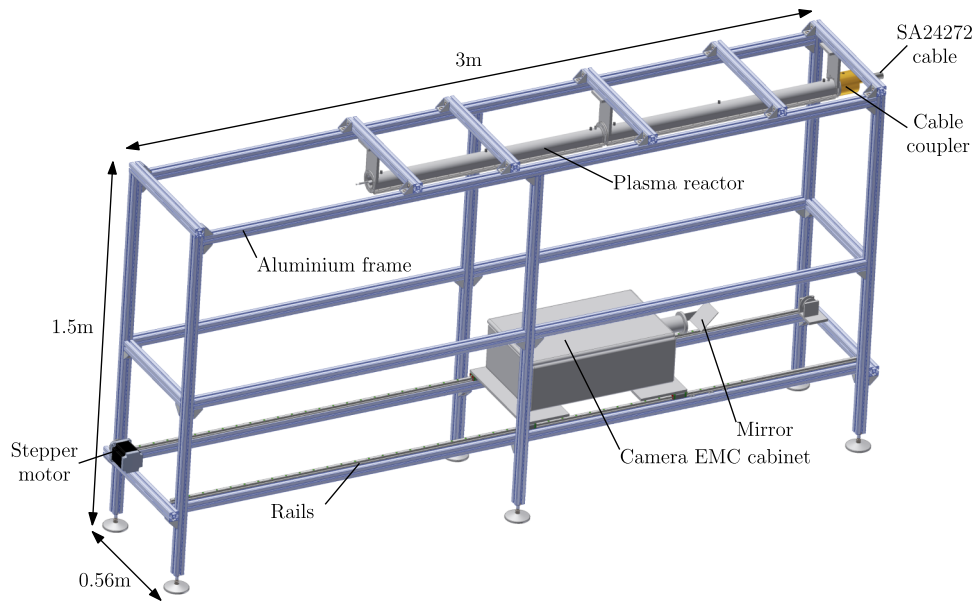
FIG. 7. A drawing of the 3-m long aluminium frame that houses the reactor and the ICCD camera. The ICCD camera is mounted in an EMC cabinet and can look at the U-shaped reactor via a mirror. The entire EMC cabinet can be moved over the length of the aluminium frame on rails. It is moved by a stepper motor that can be controlled by a computer.

B_3, and B_4, on the reactor side (see Fig. 1). Details on this measurement technique can be found in Refs. 28 and 29. The results show that the dissipated plasma energies are very similar for both reactors, with slightly less dissipation for the U-shaped reactor, as we expected.

C. Camera frame

Figure 7 shows a drawing of the entire camera frame. It is a 3-m long aluminium frame which holds all the components. Two of the U-shaped plasma reactors connected in series can be positioned on the frame, where one of the reactors can be connected to the cable coupler on the SA24272 cable. From beneath, the camera can look into the reactor via a mirror. The resulting image area of the photos is 53×71 mm^2. A stepper motor can move the camera over the rails on which the camera is mounted. In this way, nearly the entire length of the reactor can be imaged. Both the stepper motor and the camera can be fully controlled by a computer. (Unfortunately, it turned out that the very beginning of the reactor (at the side of the cable coupler) is not reached by the camera. Therefore, we are unable to image the first 12.5 cm of the reactor.)

FIG. 8. The schematic of the camera trigger circuit (with component values). It transforms the very short D-dot- or B-dot-sensor signal into a longer pulse on which the ICCD camera can trigger reliably.

D. Camera system

We used a 4 Picos-DIG ICCD camera from Stanford Computer Optics to image the streamer discharge. It has a minimum exposure time of 200 ps and its CCD has a resolution of 780×580 pixels. We attached a Sigma 70–300 F4–5.6 DG MACRO lens to the camera and enclosed it in an EMC (electromagnetic compatibility) cabinet (a shielded cabinet) to minimize the disturbance from electromagnetic interference. The EMC cabinet with the camera is mounted on the rails in the camera frame such that a stepper motor can move the camera. Furthermore, since the camera is positioned parallel to the plasma reactor, a first surface mirror is placed at a 45° angle such that the camera can look into the plasma reactor.

An important part of the camera system is the camera triggering. The internal delay of the camera is around 65 ns, but not known exactly. Therefore, to keep the SA24272 cable as short as possible, the camera should be triggered as quickly as possible after the spark gap of the nanosecond pulse source switches. If we are to achieve a 1-ns time resolution in our measurements, the jitter on the camera trigger should not exceed several hundreds of picoseconds. A suitable trigger signal can be taken from the D-dot or B-dot sensor on the pulse source side of the SA24272 cable. However, the pulses from these sensors are too short for the camera to trigger on (an example is shown further in the text). Therefore we developed a fast trigger circuit for the camera.

Figure 8 shows the trigger circuit. The circuit uses high-frequency transistors and ensures that the sensor signal initiates a longer pulse at the output of the circuit.

Figure 9 shows the input and output of the trigger circuit. It shows that the trigger circuit successfully transforms the short input pulse into a longer pulse for the camera. The circuit only triggers on the positive pulses from the sensor signal, which means that an additional delay of the duration of the pulse from the pulse source is generated in the circuit in the case of a
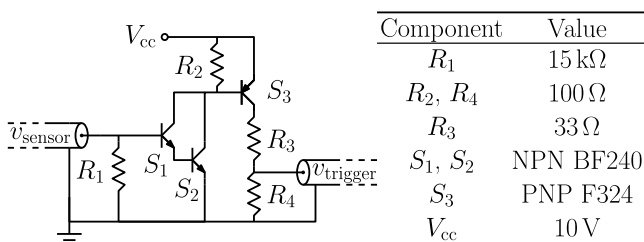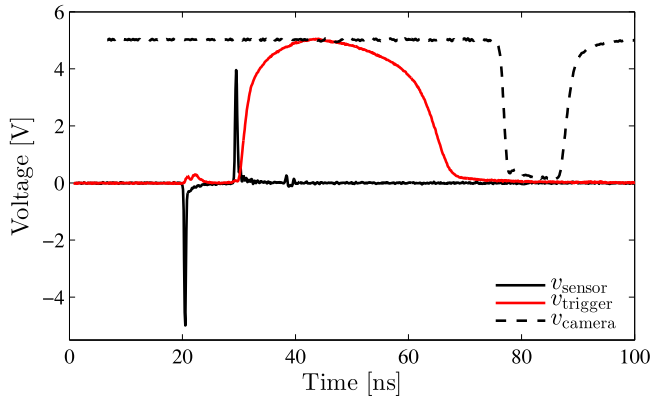
FIG. 9. The waveforms in the trigger circuit. The circuit transforms the positive peak from the sensor (v_{sensor}) into a longer pulse ($v_{trigger}$) for the ICCD camera trigger. The camera signal (v_{camera}) confirms that the camera has triggered.
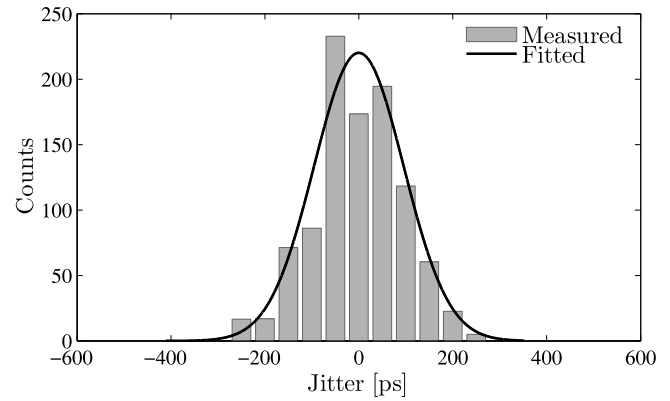

FIG. 10. A histogram of the jitter between the sensor signal and the trigger-confirmation signal of the camera. The jitter is within an acceptable range of several hundreds of picoseconds.

negative output pulse (as is the case for the signal in Fig. 9). An output on the camera shows that it has indeed triggered on the pulse from the trigger circuit. The jitter between this camera output and the sensor signal is shown in Fig. 10 for 1000 shots. The figure shows that the jitter is within the acceptable range of several hundreds of picoseconds and has a standard deviation of 95 ps.

E. Automation

The entire setup, as shown in Fig. 1, is fully automated and can be controlled by software on a computer. For each measurement we can set the number of x-positions (the physical position in the aluminium camera frame) the camera takes photos at (in steps of 5 cm), the exposure time of the camera t_e, the shutter delay of the camera t_d, the gain of the camera U_g, and the amount of photos the camera takes at each setting (usually 20). We have to adjust the nanosecond pulse source manually (spark-gap distance, PFL length, and DC-charge voltage for the pulse charger), but once it is set, the computer controls the pulse generation with the pulse charger controller.

Figure 11 shows the flowchart of the measurement control that the computer uses. The first step is that the computer resets the setup and sends the camera to the first x-position in the camera frame. It then starts taking photos at all the user-specified t_e-, t_d-, and U_g-settings before moving the camera to the next x-position. For each photo, the computer generates a

pulse with the pulse source and records the waveforms from D-dot sensors, D_3 and D_4 and B-dot sensors, B_3 and B_4 from the oscilloscope. After all the measurements for one shutter delay are complete, the computer checks if all the generated pulses by the nanosecond pulse source produced a photo and if all pulses were recorded by the oscilloscope. Sometimes this is not the case due to variable delays in the camera and oscilloscope software. If this is the case, all measurement files for that shutter delay are deleted and the measurement is repeated. In general, we record photos and voltage and current waveforms for 20 pulses at each shutter delay for average purposes. Once the measurement is complete, the computer initiates the measurement for the next shutter delay, until all delays are done. This process is then repeated for each x-position until the camera reaches the end of the aluminium frame.

F. Calibration

The system we described in Secs. II A–II E allows us to image the streamer discharge at different positions in the reactor. We stated that these images will be stitched together to form one large image of the entire reactor for one camera delay and exposure setting. This stitching is done by software and needs to be calibrated.

The calibration of the area covered per pixel is done by placing a grid with a thin line every millimeter and a thick line every centimeter onto the wire inside the reactor. The camera is focussed on this grid. The amount of pixels used to span 1 cm is counted which resulted in an area of 0.1×0.1 mm^2
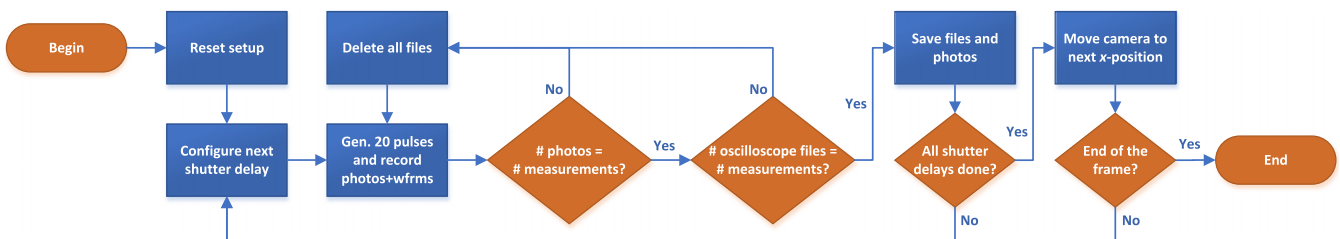

FIG. 11. Flowchart of the computer control of the measurements. The computer generates 20 pulses (for averaging purposes) with the nanosecond pulse source for each camera setting at every shutter delay and x-position that the user specified. For each pulse, a photo is taken and voltage and current waveforms are stored. It also checks if all pulses generated a photo and oscilloscope files.
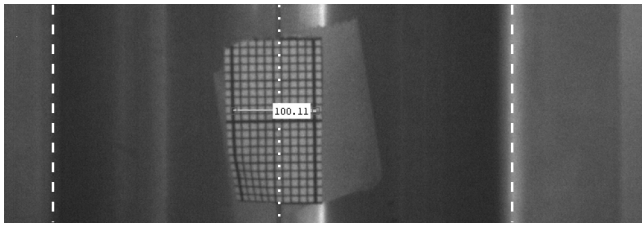
FIG. 12. Calibrating the distance spanned per pixel. A grid of 20×10 mm^2 with a thick line every 10 mm and a thin line every 1 mm is used as a reference. The label shows the amount of pixels between two thick lines, so every pixel spans a distance of 0.1×0.1 mm^2. The locations of the reactor walls (dashed) and the wire (dotted) are also given.
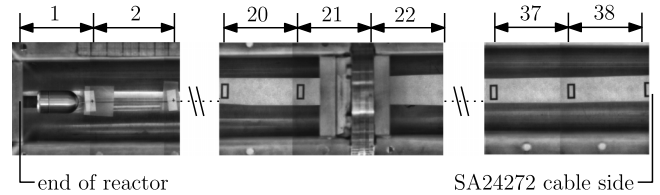

FIG. 13. An overview of the 2-m reactor and the numbering of the positions, including the squares used for calibrating and creating the stitching transformation matrix.

covered per pixel. An example of this calibration can be found in Fig. 12.

The 2-m reactor is divided into 38 sections of partially overlapping photos which are stitched together using a transformation matrix. This matrix is obtained using an image recognition script which uses evenly spaced squares attached to the wire inside the reactor. These squares and some of the positions can be found in Fig. 13.

III. DATA PROCESSING

A. Data management

The result of the automation of the entire setup is that we can perform a significant amount of experiments automatically. However, this also results in a significant amount of

data from the oscilloscope and the camera, which have to be stored and sorted. This is the first of the two steps of the data-processing process that we apply to the raw data and consists of sorting the data by its camera and experimental settings and storing the data in a MySQL database.

B. Streamer parameter calculation

Once the MySQL database is filled with the raw data of the experiment, the second step in the data processing is the calculation of the streamer parameters. These are parameters which are automatically calculated by software from the ICCD images from the MySQL database. Figure 14 shows an example of this procedure. Figure 14(a) gives a raw ICCD image with lines added by the software to indicate the reactor wall and the high-voltage wire of the reactor. The bright dots are the streamers. From the raw image, the software script determines with a brightness-threshold value in which areas the streamers are active in the top half of the image (the area below the upper reactor wall and above the high voltage (HV)

(a)

(b)
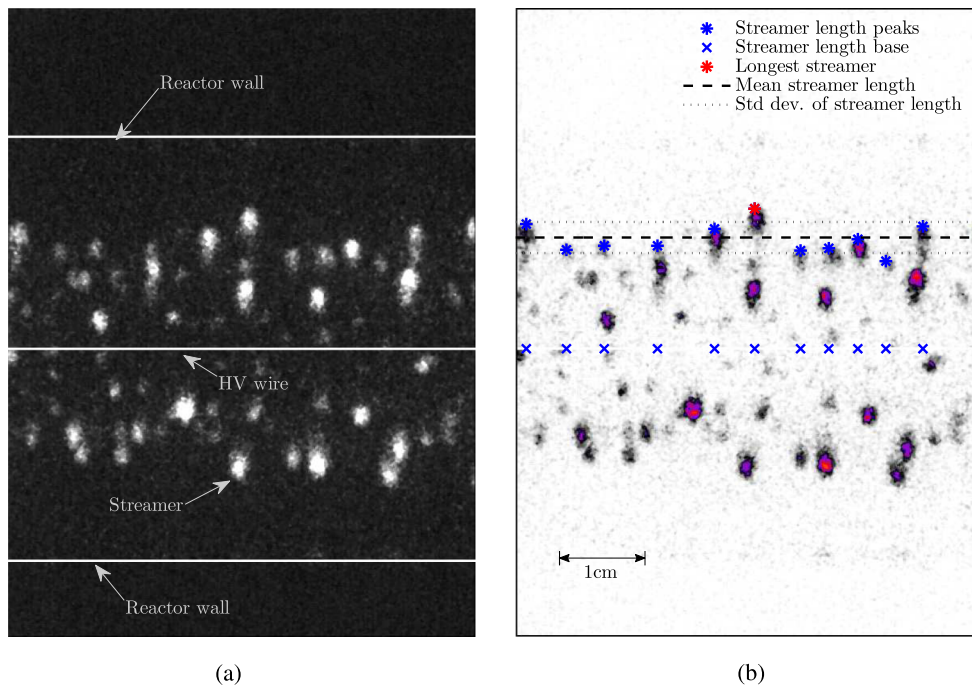
FIG. 14. An example of how the raw images are processed. The raw image in (a) is taken near the end of the reactor for a 9-ns pulse, a camera delay of 9 ns, and a voltage of 36 kV (in this example, we enhanced the contrast for clarity). In (a) the software added lines for the reactor wall and the high-voltage wire. The bright dots are the heads of the streamers. (b) The automated script detects the position of the streamers from a filtered streamer profile (see Fig. 15). This streamer profile is generated from the image by applying a brightness-threshold value above which the brightness is deemed to come from the light emission from the streamers. We applied a colour map to the raw image for clarity.
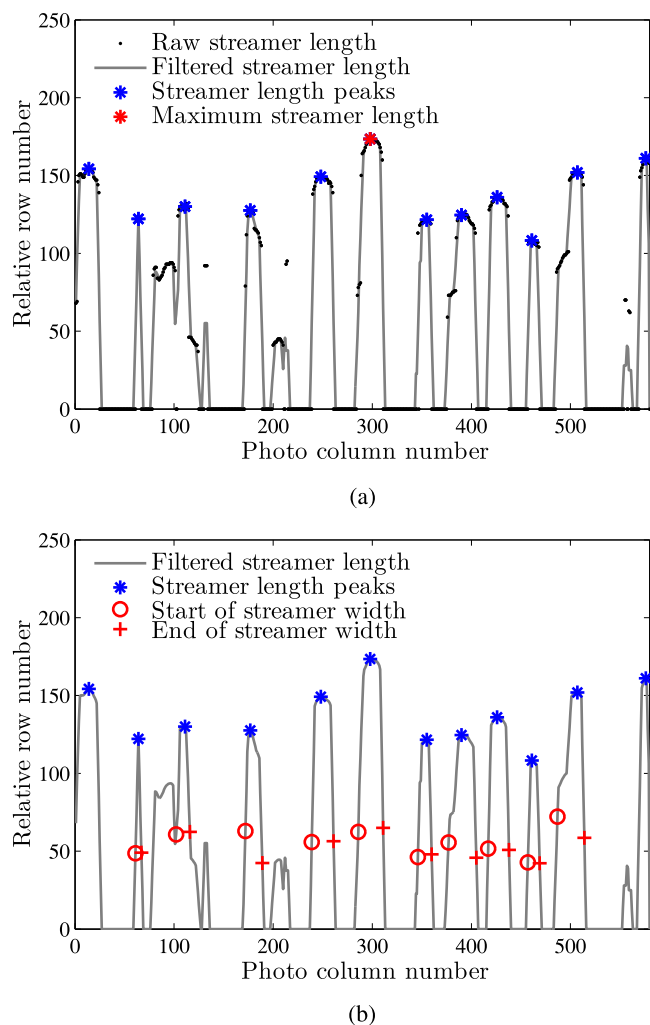
FIG. 15. (a) The streamer lengths are calculated from the filtered profile as the local maxima. The same profile is then used to calculate the streamer widths in (b) as the FWHM value of the peaks in the profile.

wire). The envelope of this active streamer area is then calculated and filtered with a moving average filter, which results in a filtered streamer profile. Figure 15(a) shows this filtered streamer profile. From the profile, the streamer lengths—the distance normal to the wire electrode that the streamer head has travelled from the high-voltage wire electrode towards the wall of the reactor—are calculated as the local maxima from the streamer profile. Subsequently, the streamer widths are calculated as the FWHM from the individual peaks (representing separate streamers) of the streamer profile. Figure 15(b) shows these streamer widths. In Fig. 14(b) we added the relevant information to the raw image (with a color map applied) to show how the calculated parameters relate to the raw data.

To ensure that we always use the streamer-length data from streamers that propagate in the plane of focus, we only take the maximum streamer length of each image to calculate the streamer lengths for a certain experimental setting. Furthermore, we use the same procedure that was used for the top half of the image to calculate the streamer parameters for the bottom half of the image (the area below the HV wire and above the bottom reactor wall).

We should mention that the method with which we calculate the streamer widths (from the streamer profiles) is not the method that should ideally be used. A more acceptable method would be the one used in Refs. 6, 12, and 13. First, we would need to isolate the head of each streamer and then calculate an intensity profile averaged along the propagation direction. From this intensity profile, the full width at half-maximum (FWHM) is then the streamer diameter. Because the method that we used in this chapter is different from the FWHM-method, the absolute value of the streamer diameters that we report may not be directly compared with other diameters reported in literature because they might be slightly different. However, the relative differences in streamer diameter that we find in our results will still be relevant. It will be left for a future update of the data processing to implement the FWHM-method for streamer-diameter determination.

Each calculated streamer parameter is again stored in the MySQL database, to be used in the presentation of the results of the experiments. Examples of calculated streamer parameters for an experiment are shown in Section IV.

C. Full-length images

Besides calculating streamer parameters from the MySQL database, another option is to generate the full-length images of the streamer discharge in the reactor for different instances of time. These images are generated by stitching the individual images (averaged over 20 images) using the calibrated stitching method from Section II F. Examples of full-length images for an experiment are shown in Section IV. Finally, movies of the streamer propagation can be generated by showing the development of the full-length images in time. An example of such a movie is added as supplementary material to this paper.

IV. EXAMPLE RESULTS

In this section, we show some example results generated with our experimental setup. In this experiment, we fix the output voltage and pulse duration of the pulse source and let the camera run through all the x-positions (in steps of 5 cm) at 1-ns exposure times with steps in the camera shutter delay of 2 ns. In this way, we get a complete time-resolved and space-resolved picture of the streamer development and propagation (not only from the wire towards the outer electrode but also the development along the wire). We set the pulse source to a high output voltage (32 kV in this case) to get the most information out of the images (if we lower the output voltage too much, there is very little to see in the images). For each camera-setting, the camera takes 20 photos so that we can average the calculated streamer parameters at each setting. This averaging is required because of the standard deviation on the output voltage of the nanosecond pulse source.[2] Ideally, we would take even more photos at each setting, but this would be extremely time consuming. Each of the automated experiments can take up to 3 h to finish when 20 photos are taken at each setting, after which it takes another hour to process the data into the MySQL database and calculate the streamer parameters.

We use the 2-m reactor in the example experiment to show the significant influence of the pulse propagation on
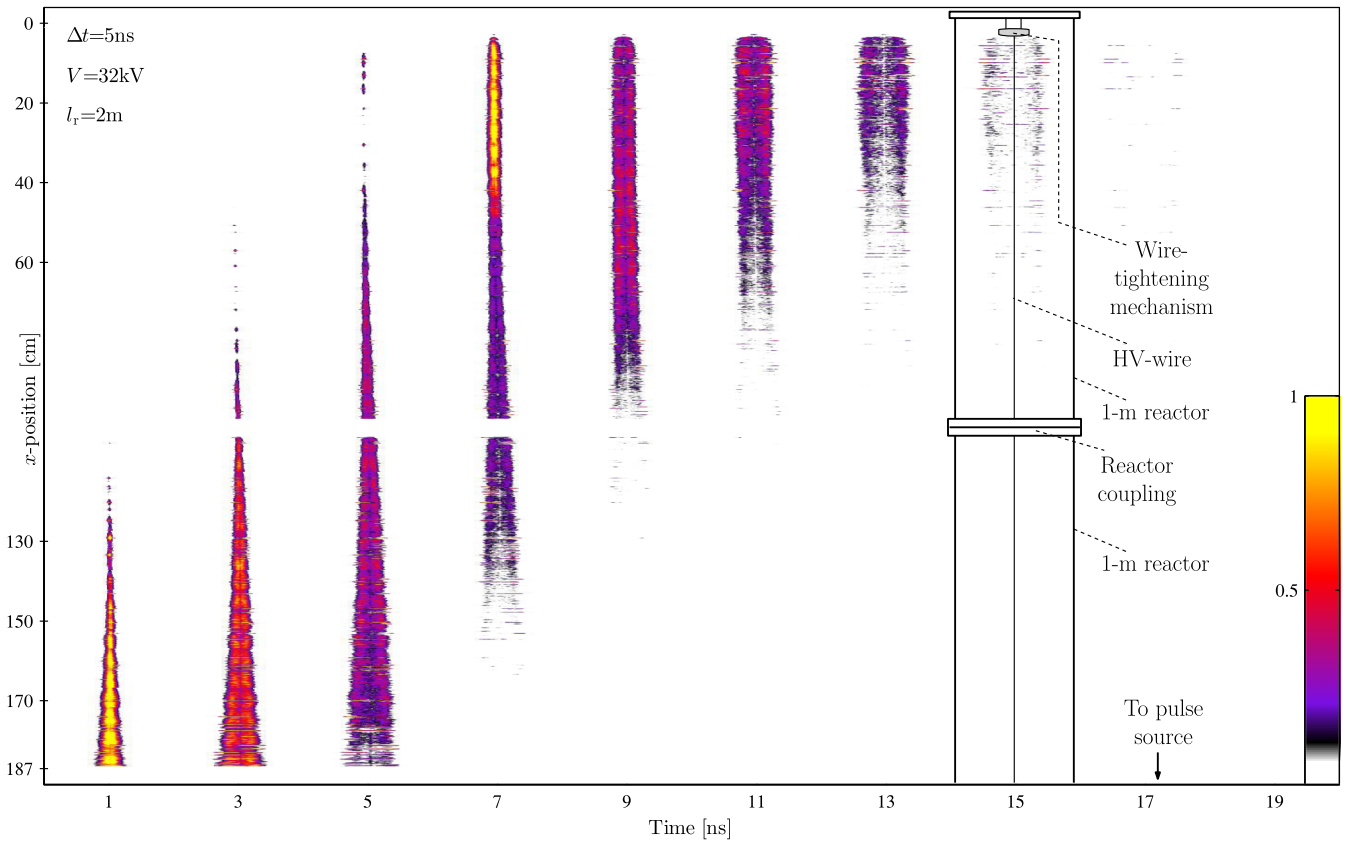
FIG. 16. Streamer development and propagation in time for a 5-ns positive pulse in a 2-m reactor. In this example, the exposure time of the ICCD camera was 2 ns. For clarity, the figure also shows how the images relate to the geometry of the reactor (shown at 15 ns). Please note that the middle of the reactor (around $x = 100$ cm) cannot be imaged due to the coupling of the two 1-m reactors.
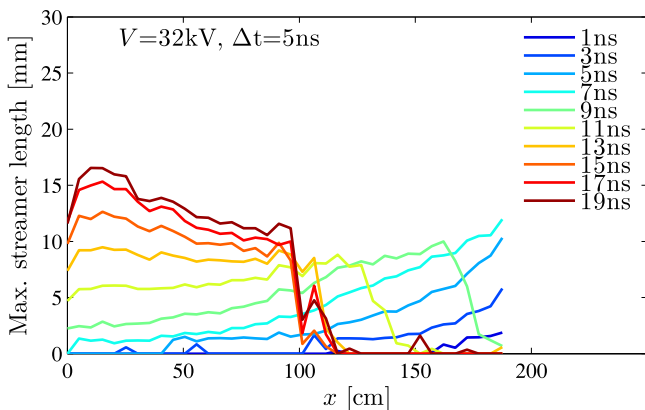

FIG. 17. Averaged (over 20 photos) maximum streamer length as a function of time (determined by the camera shutter delay) and position in the reactor calculated from the results of Fig. 16.
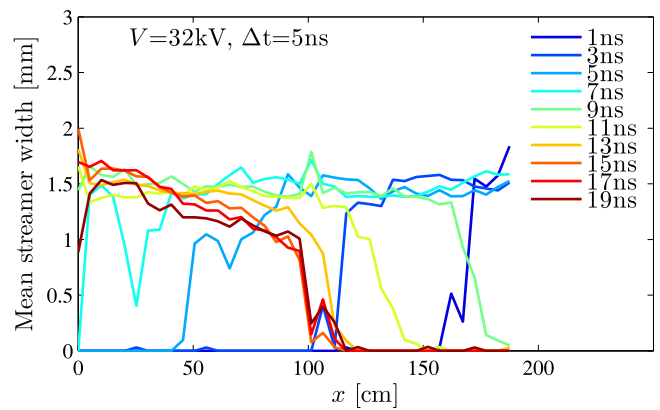

FIG. 18. Averaged (over 20 photos) mean streamer width as a function of time (determined by the camera shutter delay) and position in the reactor calculated from the results of Fig. 16.

the streamer development. Furthermore, we use a 5-ns pulse duration.

Figure 16 shows the (normalized) full-length ICCD images of the experiment for different instances in time (determined by the camera shutter delay). For clarity, the figure also shows how the images relate to the geometry of the reactor (shown at 15 ns). Please note that the middle of the reactor (around $x = 100$ cm) cannot be imaged due to the coupling of the two 1-m reactors.

The results of the experiment clearly show the propagation of the 5-ns pulse through the reactor. The resulting

streamer discharge is not evenly distributed along the wire and clearly shows longer streamers at the beginning and at the end of the reactor. At the beginning of the reactor, the pulse still has its full amplitude, but once streamers develop, the resulting dissipation attenuates the voltage amplitude of the pulse and disperses the rectangular pulse shape. As a result, at positions further from the beginning of the reactor, the streamers are shorter. At the end of the reactor, the pulses reflect because the end of the reactor is an open ended transmission line, which results in a much higher voltage at the end of the reactor and thus longer streamers.

While Fig. 16 qualitatively shows the streamer development, Fig. 17 shows the results in a quantitative way. The figure shows the average (over 20 photos) maximum streamer length as a function of time (determined by the camera shutter delay) and position in the reactor. It is one of the streamer parameters that was automatically calculated from the MySQL database. The figure shows the same results as Fig. 16 but in a much clearer way. From these results, we could, for instance, calculate the streamer velocity at different positions at different times. Figures such as Fig. 17 can further be used to quantitatively compare results of different experiments.

Finally, Fig. 18 shows the calculated mean streamer width as a function of position in the reactor and time. It shows that the streamer width is rather constant at all positions in the reactor.

V. SUMMARY

In this paper, we presented an experimental setup to image streamers in a long pulsed corona reactor as a function of time and position in the reactor. With this unique setup, we are able to follow how the propagation of a very short (sub)nanosecond high-voltage pulse influences the development and propagation of streamers in the reactor.

The setup consists of a large frame in which a specially designed plasma reactor can be suspended and imaged from below by an ICCD camera. This camera is mounted on a platform which can be moved by a stepper motor. A computer automates all the experiments. With the automated setup, we can take ICCD images of the entire plasma reactor at different instances of time and can consequently automatically calculate streamer parameters such as the streamer length and width.

We showed some example results at the end of the paper, which indicated that the streamer development and propagation depends significantly on the pulse propagation through the reactor. In a future paper, we will present a large study with the experimental setup in which we change different pulse source parameters and the length of the reactor.

SUPPLEMENTARY MATERIAL

With the information such as that of Fig. 16 we can generate movies of the streamer discharge development. We added a movie corresponding to results obtained in a 1-m reactor with positive 9-ns pulses and positive 5-ns pulses (both with a 1-ns shutter time and resolution) as online supplementary material to this paper.

ACKNOWLEDGMENTS

[1]T. Huiskamp, S. J. Voeten, E. J. M. van Heesch, and A. J. M. Pemen, "Design of a subnanosecond rise time, variable pulse duration, variable amplitude, repetitive, high-voltage pulse source," IEEE Trans. Plasma Sci. **42**, 127–137 (2014).

[2]T. Huiskamp, F. J. C. M. Beckers, E. J. M. van Heesch, and A. J. M. Pemen, "First implementation of a subnanosecond rise time, variable pulse duration, variable amplitude, repetitive, high-voltage pulse source," IEEE Trans. Plasma Sci. **42**, 859–867 (2014).

[3]T. Huiskamp, E. J. M. van Heesch, and A. J. M. Pemen, "Final implementation of a subnanosecond rise time, variable pulse duration, variable amplitude, repetitive, high-voltage pulse source," IEEE Trans. Plasma Sci. **43**, 444–451 (2015).

[4]T. Huiskamp, F. J. C. M. Beckers, E. J. M. van Heesch, and A. J. M. Pemen, "A solid state, 0–120 kV, microsecond pulse charger for a nanosecond pulse source," IEEE Trans. Plasma Sci. **41**, 3666–3674 (2013).

[5]P. P. M. Blom, "High-power pulsed corona," Ph.D. thesis, Eindhoven University of Technology, 1997.

[6]T. M. P. Briels, E. M. Van Veldhuizen, and U. Ebert, "Positive streamers in air and nitrogen of varying density: Experiments on similarity laws," J. Phys. D: Appl. Phys. **41**, 234008 (2008).

[7]P. Tardiveau, E. Marode, and A. Agneray, "Tracking an individual streamer branch among others in a pulsed induced discharge," J. Phys. D: Appl. Phys. **35**, 2823 (2002).

[8]R. Ono and T. Oda, "Formation and structure of primary and secondary streamers in positive pulsed corona discharge-effect of oxygen concentration and applied voltage," J. Phys. D: Appl. Phys. **36**, 1952 (2003).

[9]G. J. J. Winands, Z. Liu, A. J. M. Pemen, E. J. M. Van Heesch, and K. Yan, "Analysis of streamer properties in air as function of pulse and reactor parameters by ICCD photography," J. Phys. D: Appl. Phys. **41**, 234001 (2008).

[10]L. Zhao, Z. Y. Luo, J. Y. Xuan, J. P. Jiang, X. Gao, and K. F. Cen, "Study of geometry structure on a wire–plate pulsed corona discharge reactor," IEEE Trans. Plasma Sci. **40**, 802–810 (2012).

[11]A. V. Krasnochub, M. M. Nudnova, and A. Y. Starikovskii, "Cathode-directed streamer development in air at different pressures," AIAA Paper 2005-203 (2005).

[12]S. Nijdam, F. M. J. H. Van De Wetering, R. Blanc, E. M. Van Veldhuizen, and U. Ebert, "Probing photo-ionization: Experiments on positive streamers in pure gases and mixtures," J. Phys. D: Appl. Phys. **43**, 145204 (2010).

[13]T. M. P. Briels, J. Kos, G. J. J. Winands, E. M. Van Veldhuizen, and U. Ebert, "Positive and negative streamers in ambient air: Measuring diameter, velocity and dissipated energy," J. Phys. D: Appl. Phys. **41**, 234004 (2008).

[14]T. Namihira, D. Wang, S. Katsuki, R. Hackam, and H. Akiyama, "Propagation velocity of pulsed streamer discharges in atmospheric air," IEEE Trans. Plasma Sci. **31**, 1091–1094 (2003).

[15]D. Wang, M. Jikuya, S. Yoshida, T. Namihira, S. Katsuki, and H. Akiyama, "Positive-and negative-pulsed streamer discharges generated by a 100-ns pulsed-power in atmospheric air," IEEE Trans. Plasma Sci. **35**, 1098–1103 (2007).

[16]H.-H. Kim, "Nonthermal plasma processing for air-pollution control: A historical review, current issues, and future prospects," Plasma Processes Polym. **1**, 91–110 (2004).

[17]A. Fridman, A. Chirokov, and A. Gutsol, "Non-thermal atmospheric pressure discharges," J. Phys. D: Appl. Phys. **38**, R1 (2005).

[18]S. Samukawa, M. Hori, S. Rauf, K. Tachibana, P. Bruggeman, G. Kroesen, J. C. Whitehead, A. B. Murphy, A. F. Gutsol, S. Starikovskaia, U. Kortshagen, J. Boeuf, T. J. Sommerer, M. J. Kushner, U. Czarnetzki, and N. Mason, "The 2012 plasma roadmap," J. Phys. D: Appl. Phys. **45**, 253001 (2012).

[19]T. Huiskamp, "Nanosecond pulsed power technology for transient plasma generation," Ph.D. thesis, Eindhoven University of Technology, 2015, available online: https://pure.tue.nl/ws/files/3809268/798746.pdf.

[20]E. J. M. van Heesch, G. J. J. Winands, and A. J. M. Pemen, "Evaluation of pulsed streamer corona experiments to determine the O* radical yield," J. Phys. D: Appl. Phys. **41**, 234015 (2008).

[21]T. Matsumoto, D. Wang, T. Namihira, and H. Akiyama, "Energy efficiency improvement of nitric oxide treatment using nanosecond pulsed discharge," IEEE Trans. Plasma Sci. **38**, 2639–2643 (2010).

[22]D. Wang, T. Namihira, and H. Akiyama, "Recent progress of nano-seconds pulsed discharge and its applications," J. Adv. Oxid. Technol. **14**, 131–137 (2011).

[23]T. Matsumoto, D. Wang, T. Namihira, and H. Akiyama, "Process performances of 2 ns pulsed discharge plasma," Jpn. J. Appl. Phys., Part 1 **50**, 08JF14 (2011).

[24]M. Fujiwara, "Short-pulse discharge for simultaneous pursuit of energy and volume-efficient NO_x removal," Jpn. J. Appl. Phys., Part 1 **45**, 948 (2006).

[25]T. Kakuta, I. Yagi, and K. Takaki, "Improvement of deoxidization efficiency of nitric monoxide by shortening pulse width of semiconductor opening

switch pulse power generator," Jpn. J. Appl. Phys., Part 1 **54**, 01AG02 (2015).

[26] R. Ono, Y. Nakagawa, and T. Oda, "Effect of pulse width on the production of radicals and excited species in a pulsed positive corona discharge," J. Phys. D: Appl. Phys. **44**, 485201 (2011).

[27] T. Namihira, S. Tsukamoto, D. Wang, S. Katsuki, R. Hackam, H. Akiyama, Y. Uchida, and M. Koike, "Improvement of NO_x removal efficiency using short-width pulsed power," IEEE Trans. Plasma Sci. **28**, 434–442 (2000).

[28] T. Huiskamp, F. J. C. M. Beckers, E. J. M. van Heesch, and A. J. M. Pemen, "B-dot and d-dot sensors for (sub)nanosecond high-voltage and high-current pulse measurements," IEEE Sens. J. **16**, 3792–3801 (2016).

[29] T. Huiskamp, F. J. C. M. Beckers, W. F. L. M. Hoeben, E. J. M. van Heesch, and A. J. M. Pemen, "Matching a (sub)nanosecond pulse source to a corona plasma reactor," Plasma Sources Sci. Technol. **25**, 054006 (2016).